Antarct. Meteorite Res., **18**, 17–45, 2005

Mineralogy of Yamato 983885 lunar polymict breccia with a KREEP basalt, a high-Al basalt, a very low-Ti basalt and Mg-rich rocks

Tomoko Arai[1*†], Mayumi Otsuki[2], Teruaki Ishii[2], Takashi Mikouchi[3] and Masamichi Miyamoto[3]

[1]*Lunar Exploration Technology Office, Japan Aerospace Exploration Agency (JAXA), 2–1–1, Sengen, Tsukuba 305-8505*
[2]*Ocean Research Institute, The University of Tokyo, Minamidai, Nakano-ku, Tokyo 164-8639*
[3]*Department of Earth and Planetary Science, The University of Tokyo, Hongo, Bukyo-ku, Tokyo 113-0033*
[*]*Present address: Antarctic Meteorite Research Center, National Institute of Polar Research (NIPR), Kaga 1-chome, Itabashi-ku, Tokyo 173-8515*
[†]*Corresponding author. E-mail: tomoko@nipr.ac.jp*

(Received September 30, 2004; Accepted February 7, 2005)

Abstract: Y983885 is a polymict regolith breccia with a KREEP basalt, Mg-rich troctolite/norite, a high-Al basalt, a very low-Ti basalt, a granulite originated from ferroan anorthosite, and Si, Na-rich impact spherules. An igneous KREEP basalt is first reported among lunar meteorites to date. The KREEP basalt is mineralogically distinct from Apollo KREEP basalts due to the lack of the typical Ca zoning from orthopyroxene to pigeonite, instead, the presence of the co-existing pigeonite/augite with chemical zonings and micron-scale exsolution. With these mineral characteristics, the KREEP basalt is probably cooled slightly slower than the Apollo KREEP basalts under the subsurface condition such as hypabyssal setting or lava pond. Further study of the additional samples is necessary to fully understand the petrogenesis of this new KREEP basalt. The troctolite and norite are also distinct in lower mg# of mafic minerals and higher modal abundance of olivine in norite, comparing to Apollo troctolites and norites, implying the existence of a rock type with intermediate modal abundance between norite and troctolite, and the compositional diversity of Mg-rich lithologies. Simultaneous occurrence of a KREEP basalt and a genetically KREEP-related, high-Al basalt, a Mg-rich troctolite/norite and the Si, Na-rich impact glasses can constrain the source region of Y983885 to the KREEP-rich Procellarum terrane in the northwestern hemisphere of the lunar nearside.

key words: lunar meteorite, KREEP, Mg-rich rock, high-Al basalt, very low-Ti basalt

1. Introduction

Mineralogical study of breccias is crucial to understand the lunar crust, because the intense heavy bombardment of the Moon which probably terminated at around 3.95 Ga obscures the record of crustal formation and evolution in the earlier history of the Moon. Almost all the highland rock samples which are considered to constitute the lunar crust are heavily brecciated and record shock effect to various extents. These crustal rock samples are much less abundant both in the number and the size, compared

to mare basalts, since they are generally found as mm-scale lithic clasts in the brecciated rocks. Evidence for the crustal evolution and ancient (crypto-mare) lunar volcanism can be studied only by remnants of crustal rocks incorporated and preserved in the regolith and regolith breccias.

Based on the studies of these brecciated samples, major constituents of the lunar crust are generally classified as following three rock types; (1) Ferroan anorthosites, (2) Mg-rich rocks (dunite, norite, troctolite, gabbronorite), (3) Alkali-rich rocks (alkali anorthosite, alkali norite, alkali gabbronorite, KREEP (enriched in K, REE and P) basalts, quartz monzodiorite, granite and felsite) (*e.g.,* Papike *et al*., 1998). While ferroan anorthosites are produced by floatation directly in the magma ocean, Mg-rich rocks and alkali-rich rocks are probably be secondary products after the magma ocean are solidified, because of the enriched incompatible element abundances, primitive (Mg-rich) mafic mineral compositions and younger crystallization ages than those of ferroan anorthosites (*e.g.*, Papike *et al*., 1998). Especially due to the unique mineralogical/geochemical characteristics, petrogenesis of the Mg-rich and Alkali-rich rock is still in debate. Assimilation of KREEP by Mg-rich magma or metasomatism of KREEPy liquid by Mg-rich pluton (intrusion) are currently the two most feasible petrogenesis models for Mg-rich rocks (Papike *et al*., 1994, 1996; Snyder *et al*., 1995a; Shervais and McGee, 1998). Alkali-rich rocks have been proposed to be cumulate rocks from KREEP basalt magma (Jolliff, 1991; Marvin *et al*., 1991; Snyder *et al*., 1995b; Shervais and McGee, 1999). However, more samples are needed to constrain further the petrogenesis of Mg-rich rocks and alkali-rich rocks and the genetic relationship with KREEP.

Yamato (Y) 983885 is a lunar-meteorite breccia recently found in Antarctica. Kaiden and Kojima (2002) reported a preliminary result of the petrography and oxygen isotopic composition, and verified its lunar derivation. The lunar meteorite is expected to provide us with an important data to understand KREEP volcanism, the petrogenesis of Mg-rich rocks and alkali-rich rocks and its relation to the KREEP, because it contains a variety of the crustal rocks, such as Mg-rich rocks and a KREEP basalt. This paper presents mineralogy of Y983885, focusing on the clast components, and discuss the petrogenesis and the association with KREEP, based on the new data set, and proposes the possible source region on the Moon.

2. Sample and method

A polished thin section (PTS) Y983885,59-2 is provided by the National Institute of Polar Research (NIPR). Chemical compositions of minerals and glasses were analyzed by a JEOL 733 electron probe microanalyzer (EPMA) and JEOL EPMA (8900 Super Probe) at the Ocean Research Institute, the University of Tokyo, and Field Emission SEM at Department of Earth and Planetary Science, the University of Tokyo. All mineral analyses were done using wavelength dispersive spectrometers operating 15 kV accelerating voltage, a 12 nA beam current and a focused beam. A combination of silicate and oxide mineral standards was used for calibration of silicates and oxides, and a correction method of Bence and Albee (1968) was used. Modal abundances of each clast were obtained by a digital processing of elemental maps using software named

Scion Images. Concentrations of Y, La, Ce, Nd, F, Cl are analyzed by JEOL EPMA (8900 Super Probe) at the Ocean Research Institute, the University of Tokyo. For the analyses of FeNi metal and troilite, FeO, NiO, pentrandite, S metal are used as standards and ZAF oxide correction were applied. Analytical standards for Y, La, Ce, Nd, F, and Cl are YPO_4, $LaPO_4$, $CePO_4$, $NdPO_4$, CaF_2, and tugutupite, respectively and ZAF oxide correction is applied.

3. Results

A polished thin section (PTS) Y983885,59-2 is a polymict regolith breccia with various types of rock clasts, isolated mineral fragments, and glass spherules, embedded in the dark glassy matrix (Fig. 1). This regolith breccia shows compact matrix, which are commonly observed in regolith breccias. Dominant dark glassy matrix is anorthositic and the population of lithic clasts is low. Fusion crust is not found in this PTS. Compared to several large clasts larger than 0.5 mm across, most of isolated mineral fragments are smaller than 100 μm in size. These mineral fragments are plagioclase, pyroxene and olivine with minor silica mineral, ilmenite, chromite, metallic Fe, and troilite. Note that isolated pyroxene fragments are finely exsolved in a few micron scales. Feldspathic impact glass spherules of 50–500 μm in diameter are found. Some

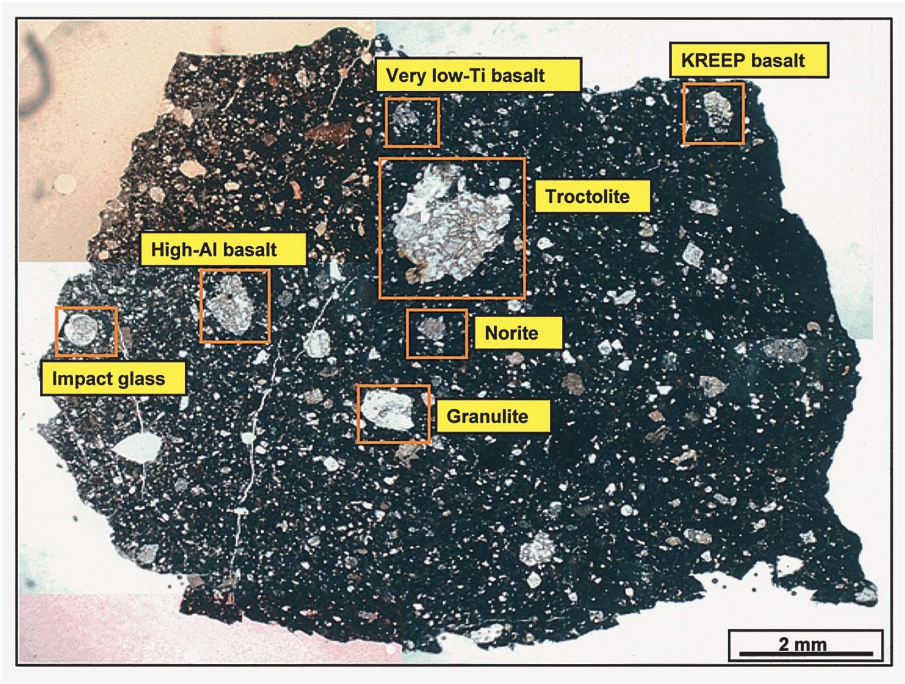

Fig. 1. Photomicrograph of a polished thin section Y983885,59-2. Various clasts and mineral fragments are embedded in the dark glassy matrix. Each clast discussed in this paper is shown by square frames.

Table 1. Modal abundance of each clast in Y983885,59-2.

	KREEP basalt	Norite	Troctolite	Granulite	Hi-Al basalt	VLT basalt
Plagioclase	64.1	48.8	59.6	91	75.4	42.5
Pyroxene	20.1	40.4	15.5	-	10.6	53.4
Olivine	-	10.8	23.4[+]	9	10.9	Tr*[1]
Ilmenite	2.1	-	-	-	-	Tr*[1]
Chromite	-	-	Tr	-	-	-
K-feldspar	Tr	-	-	-	-	-
Silica	-	-	-	-	-	4.1*[1]*[2]
SiAlK glass	10.9	-	-	-	-	-
FeS	-	-	Tr	-	1.9	-
FeNi	-	-	1.5	-	0.8	-
Whitlockite	2.8	-	-	-	-	-
Apatite	-	-	Tr	-	0.4	-

Tr = trace (less than 0.1 vol %). [+] Trace of fayalite is found around FeNi.

*[1] Fayalite, ilmenite and silica co-exist in symplectites.

*[2] Apart from symplectic silica minerals, isolated crystals of silica are also present.

glasses are devitrified and include plagioclase and pyroxene crystals, while others are fairly homogeneous. No pyroclastic glass is recognized. A variety of lithic clasts are mostly derived from highland lithologies with an exception of one probable mare basalt clast. The lithic clasts are a KREEP basalt, a Mg-rich norite, a Mg-rich troctolite, a granulite, a high-aluminum (high-Al) basalt and a very low Ti (VLT) basalt. Modal abundance of each clast is listed in Table 1. Mineralogy of each clast is presented as follows:

3.1. KREEP basalt

A clast, 0.8×0.4 mm in size, preserves a primary igneous texture with medium grain size (Fig. 2a), although the plagioclase grains show shock-induced undulatory extinction. The texture of the clast is hard to be clearly defined because the size of the

Fig. 2 (opposite).

a. Photomicrograph of KREEP basalt. The primary igneous texture is well preserved without granulation.

b. Na map of KREEP basalt. Euhedral plagioclases with extensive core-rim zoning form continuous network of laths. Compared to the large grain size (up to 200 μm), the rims of all plagioclase grains are thin (10–30 μm across).

c. Fe map of KREEP basalt. Three grains of pyroxene and ilmenite laths are shown. While Px 1 shows gradational zoning, Px 2 and Px 3 are co-existing pigeonite and augite.

d. Ca map of KREEP basalt. Co-existing high-Ca pyroxenes and low-Ca pyroxenes are found in the three pyroxene grains.

e. K map of KREEP basalt. The Si, Al, K-rich glass coexists with the extremely Na, K-rich plagioclase, Fe-rich augite (Px 2) rim and ilmenite. The Si, Al, K-rich glass is also found as droplets (about 10 μm in diameter) within REE-rich whitlockite.

f. P map of KREEP basalt. Elongated whitlockite is present with inclusions of Si, Al, K-rich glasses.

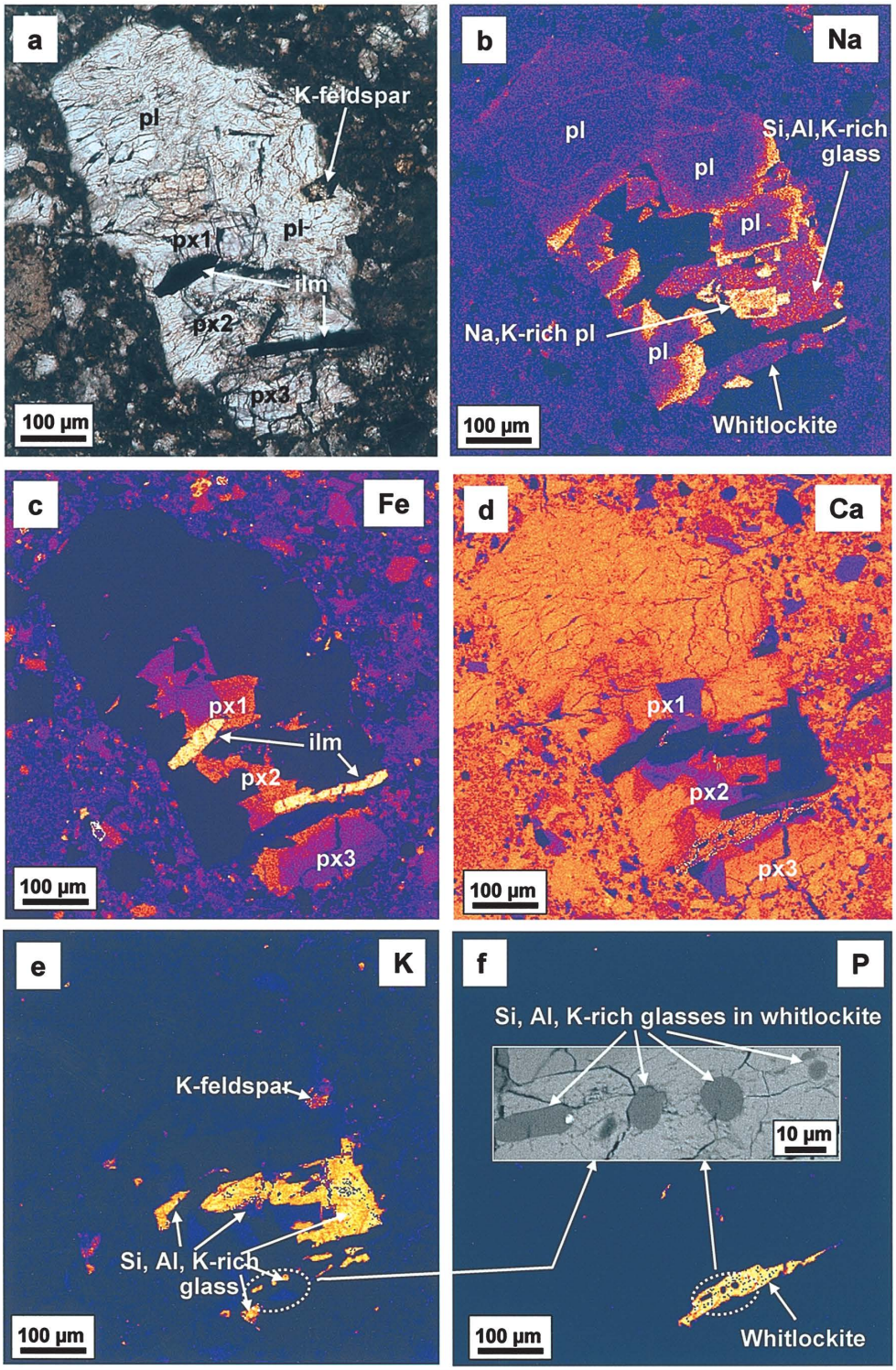
a
pl
K-feldspar
pl
px1
pl
ilm
px2
px3
100 µm
b
Na
pl
Si,Al,K-rich glass
pl
pl
Na,K-rich pl
pl
Whitlockite
100 µm
c
Fe
px1
ilm
px2
px3
100 µm
d
Ca
px1
px2
px3
100 µm
e
K
K-feldspar
Si, Al, K-rich glass
100 µm
f
P
Si, Al, K-rich glasses in whitlockite
10 µm
100 µm
Whitlockite

Table 2. Mineral compositions of KREEP basalt.

	Plagioclase				Pyroxene						Ilmenite	K-feldspar	Si, Al, K-glass		Whitlockite	
	Pl 1		Pl 2		Px 1		Px 2		Px 3							
	core	rim	core	rim	high-Ca	low-Ca	high-Ca	low-Ca	high-Ca	low-Ca						
SiO_2	44.5	50.5	51.4	55.8	52.4	52.6	51.3	50.3	52.2	49.2	0.00	59.7	76.8	79.8	SiO_2	0.21
TiO_2	0.00	0.13	0.07	0.08	1.34	0.73	1.15	1.16	1.15	1.12	52.2	0.12	0.75	0.62	TiO_2	0.00
Al_2O_3	35.4	30.6	29.3	28.7	2.01	0.74	1.27	0.89	2.18	1.24	0.07	19.6	12.7	10.7	Al_2O_3	0.41
FeO	0.16	1.53	0.66	0.69	14.2	23.2	23.4	30.5	10.5	26.5	45.2	1.67	1.18	0.87	FeO	2.65
MnO	0.00	0.00	0.01	0.02	0.36	0.43	0.32	0.56	0.25	0.51	0.41	n.d.	0.06	0.03	MnO	n.d.
MgO	0.12	0.07	0.08	0.07	15.0	17.1	11.2	10.9	15.4	10.4	1.00	0.02	0.07	0.05	MgO	1.99
CaO	19.2	14.0	13.4	12.0	15.1	5.15	12.1	6.09	17.5	9.19	0.16	0.37	0.74	0.62	CaO	43.1
Na_2O	0.45	2.94	3.20	3.87	0.10	0.05	0.07	0.08	0.08	0.06	0.00	1.14	1.30	0.90	Na_2O	0.47
K_2O	0.05	0.31	0.44	0.57	n.d.	n.d.	0.02	0.03	0.01	0.02	0.00	11.9	6.21	6.43	K_2O	0.03
Cr_2O_3	0.00	0.00	0.00	0.05	0.75	0.36	0.35	0.24	0.87	0.30	0.55	n.d.	n.d.	n.d.	Cr_2O_3	n.d.
V_2O_3	n.d.	n.d.	n.d.	n.d.	0.01	0.01	n.d.	0.03	0.04	n.d.	n.d.	n.d.	n.d.	0.01	V_2O_3	n.d.
NiO	0.00	0.00	0.00	0.04	0.01	0.04	0.01	0.01	0.00	n.d.	n.d.	n.d.	n.d.	0.00	NiO	n.d.
P_2O_5	0.00	0.10	0.11	0.11	n.d.	n.d.	n.d.	0.06	0.05	0.09	0.01	n.d.	0.18	0.14	P_2O_5	44.7
BaO	n.a.	n.a.	n.a.	n.a.	n.a.	n.a.	n.a.	n.a.	n.a.	n.a.	n.a.	4.89	n.a.	n.a.	BaO	n.a.
Total	99.9	100.2	98.7	102.0	101.3	100.5	101.0	100.9	100.2	98.7	99.5	99.5	100.0	100.2	Y_2O_3	1.15
															La_2O_3	0.69
mg#					65.2	56.8	46.0	39.0	72.3	41.2	3.8				Ce_2O_3	1.90
Wo					32.2	10.9	26.3	13.5	37.1	20.7					Nd_2O_3	1.05
Fs					23.6	38.5	39.8	52.7	17.4	46.6					Total	98.3
En					44.2	50.6	33.9	33.8	45.5	32.7						
Or	0.3	1.9	2.6	3.5								85.4				
Ab	4.1	27.1	29.4	35.6								12.4				
An	95.6	71.0	68.0	61.0								2.2				

mg# = 100 × Mg/(Mg + Fe) mol ratio, Wo = 100 × Ca/(Ca +Fe +Mg) mol ratio, Fs = 100 × Fe/(Ca + Fe + Mg) mol ratio, En = 100 × Mg/(Ca + Fe + Mg) mol ratio
Or = 100 × K/(K + Ca + Na) mol ratio, Ab = 100 × Na/(K + Ca + Na) mol ratio, An = 100 × Ca/(K + Ca + Na) mol ratio. n.d. = not detected, n.a. = not analyzed.

clast is too small to represent the original rock, but is likely subophitic. It consists of 64 vol% ternary plagioclase, 20 vol% pyroxene (pigeonite and augite), 2.8 vol% REE-rich whitlockite, 2.1 vol%, ilmenite, 11 vol% Si, Al, K-rich glass, and trace of Ba-rich potassium feldspar (Fig. 2b–f; Table 1). Mineral compositions are given in Table 2. Euhedral plagioclase grains forming continuous network of laths partly enclose pyroxene, whitlockite and ilmenite. The plagioclase shows extensive chemical zoning from core ($An_{96}Ab_4Or_0$) to rim ($An_{71}Ab_{27}Or_2$) (Fig. 3d). The rims constitute about 10–30 μm from the grain edge with abrupt discontinuity from the cores (Fig. 2b). One grain co-existing with Si, Al, K-rich glass is extremely enriched in sodium and potassium ($An_{68}Ab_{29}Or_3$–$An_{61}Ab_{36}Or_3$) (Fig. 3d). The extremely Na-rich plagioclase is apparently a product of the very last stage of the fractional crystallization. The wide-range compositional zoning probably reflects rapid cooling from a small amount of the last dreg of the melt, of which composition was successively changing with the plagioclase crystal growth.

Three grains of pyroxenes consist of high-Ca pyroxene and low-Ca pyroxene respectively (Fig. 2c and d; Fig. 4a–c). Their compositions in three grains fall within a similar range, but vary between grains (Fig. 3a–c). The most Mg-rich grain (Px 1) includes co-existing pigeonite and augite, both of which show compositional zonings. They are dominantly enclosed by plagioclases and partly coexist with ilmenite and Si, Al, K-rich glass. The pigeonite compositions represent an enrichment of Fe and Ca ($Wo_8Fs_{37}En_{55}$, mg# = 60 to $Wo_{13}Fs_{51}En_{36}$, mg# = 41) from the grain boundary with the augite to the pigeonite rim. The augite compositions change with a Fe enrichment and Ca depletion ($Wo_{37}Fs_{17}En_{46}$, mg# = 63 to $Wo_{20}Fs_{42}En_{38}$, mg# = 47) from the grain boundary with the pigeonite to the augite rim. Note that the Ca contents do not change much both in the pigeonite and augite. The less Ca-rich augites ($Wo_{18}Fs_{46}En_{36}$, mg# = 44) are found about 10 μm from the rim where the compositions discontinuously change.

The most Fe-rich pyroxene grain (Px 2) contains low-Ca pyroxene (pigeonite and augite) ($Wo_{19}Fs_{45}En_{36}$, mg# = 44 to $Wo_{12}Fs_{54}En_{34}$, mg# = 39) and augite ($Wo_{35}Fs_{33}En_{32}$, mg# = 49 to $Wo_{28}Fs_{39}En_{33}$, mg# = 46). The augite represents a compositional trend of Ca depletion toward the grain boundary with low-Ca pyroxene, while a systematic compositional change is not recognized in the low-Ca pyroxene due to the irregular grain shape. The Px 2 is found in a direct contact with the extremely Na-rich plagioclase and the Si, Al, K-rich glass.

The largest pyroxene grain (Px 3) of 200 μm-across, consists of an augite (160 μm across) mantled by a low-Ca pyroxene (up to 40 μm across), coexisting with whitlockite, plagioclase and Si, Al, K-rich glass. The augite shows a compositional trend of Ca-depletion and Fe-enrichment ($Wo_{37}Fs_{17}En_{46}$, mg# = 73 to $Wo_{26}Fs_{35}En_{39}$, mg# = 53) toward the grain boundary with the low-Ca pyroxene. The low Ca-pyroxene shows Ca and Fe enrichment from the boarder with the augite toward the grain edge ($Wo_{10}Fs_{45}En_{45}$, mg# = 50 to $Wo_{22}Fs_{46}En_{32}$, mg# = 41).

Exsolution lamellae in the three pyroxene grains are resolved both in pigeonite and augite in submicron to a few micron scales (Fig. 5). The compositions of the three pyroxene grains are partly overlapped with one another and the consolidated composition represents high-Ca pyroxenes (augites) and low-Ca pyroxene (pigeonite and augite)

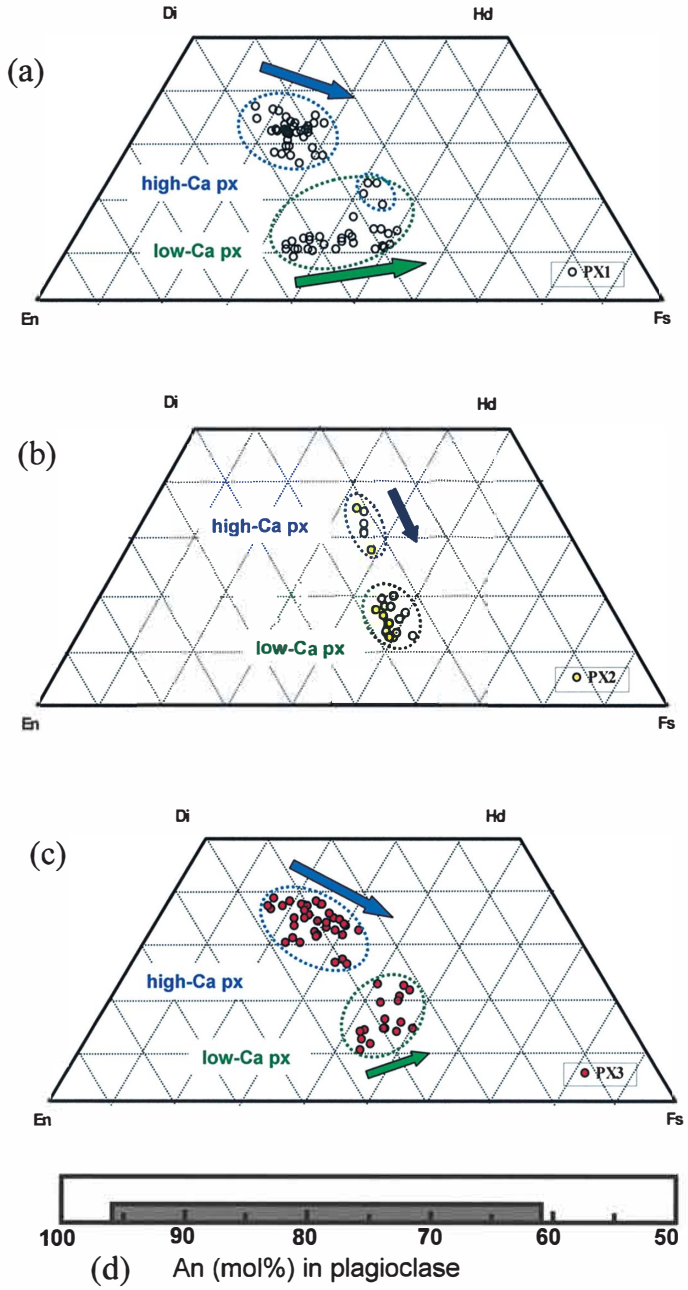

Fig. 3a–c. Pyroxene composition of KREEP basalt plotted in the pyroxene quadrilateral. While Px 1 and Px 3 show high-Ca pyroxenes with Fe-enrichment and Ca-depletion, and low-Ca pyroxenes with Fe and Ca enrichment. Low-Ca pyroxene of Px 3 shows a compositional clustering, while high-Ca pyroxene shows Ca-depletion trend.

Fig. 3d. Plagioclase composition of KREEP basalt. Plagioclasse are zoned to an extremely Na-rich composition.

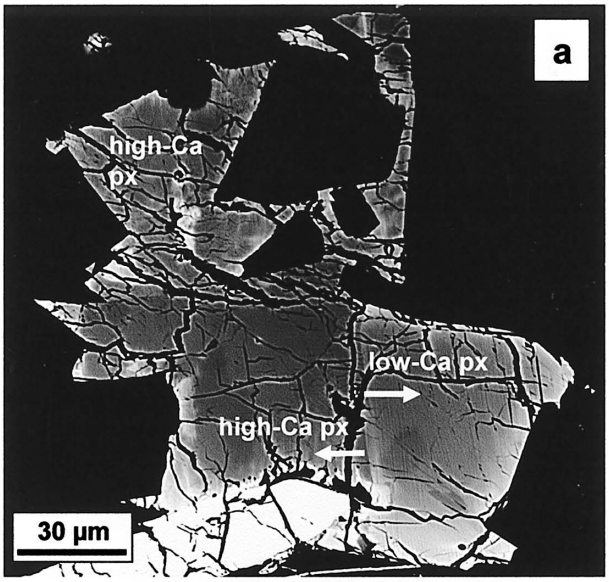

Fig. 4a. Back scattered elecrotn (BSE) image of Px 1 showing co-existing pigeonite and augite with chemical zonings toward the rim. Relatively low-Ca pyroxene are found at the edge of high-Ca pyroxene.

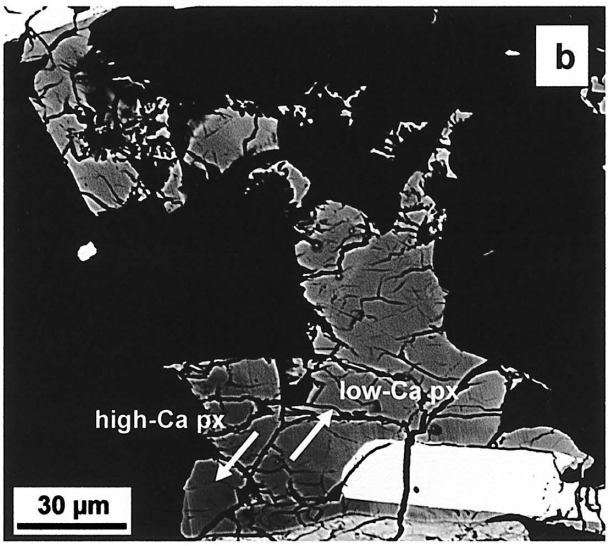

Fig. 4b. BSE image of Px 2 showing co-existing pigeonite and augite. The boundary of two pyroxene is not clear compared to Px 1 and Px 3.

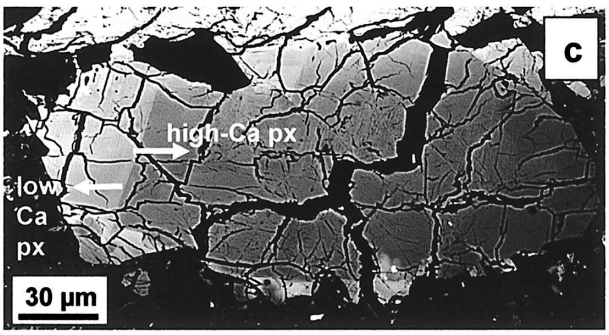

Fig. 4c. BSE image of Px 3 showing high-Ca core and low-Ca rim. Chemical zoning in the high-Ca pyroxene (from right to left) toward the boundary with low-Ca pyroxene is visible.

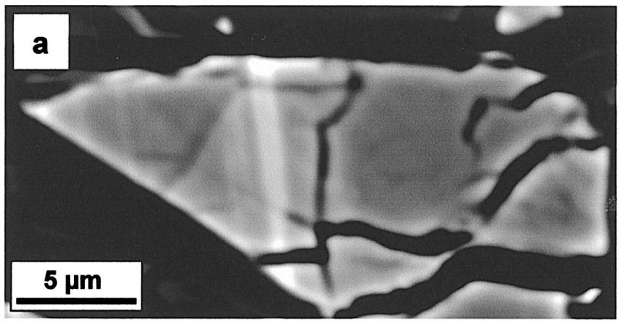

Fig. 5a. BSE image of exsolved pigeonite (light gray) in host augite (dark gray). The thickness of lamella is about 1 μm.

Fig. 5b. BSE image of exsolved augite (dark gray) in host pigeonite (light gray). Note that the thickness of lamella ranges from submicron-scale to 3 μm.

both of which compositions have a series of zoning trends of Fe-enrichment and Ca-depletion/enrichment respectively, starting with Px 1, followed by Px 3 and Px 2. The difference of the pyroxene compositions in the three grains might be due to the unrepresentative data from the limited cut surface of the small clast, but could also represent the crystallization sequence (Px 1→Px 3→Px 2) from a small volume of the melt at the late-stage of the fractional crystallization, where a precipitation of a small mineral grain can drive a dramatic change of the melt composition. The Ti/Al values are 0.33–0.66 in Px 1, 0.53–0.83 in Px 2, and 0.34–0.63 in Px 3, which indicates crystallization of all the three pyroxenes after plagioclase saturation (Bence and Papike, 1972).

The Si, Al, K-rich glass coexists with the extremely Na, K- rich plagioclase, Fe-rich augite (Px 2) rim and ilmenite (Fig. 2b and c). The glass is compositionally heterogeneous (SiO_2=76.4–80.1 wt%, K_2O=5.14–6.46 wt%, Al_2O_3=10.7–12.7 wt%) and contains up to 5 wt% of BaO (Table 2). The Si, Al, K-rich glass is also found as droplets (about 10 μm in diameter) within REE-rich whitlockite (Fig. 2f). This indicates that the Si, Al, K-rich liquid was generated upon the whitlockite precipitation in the fractional crystallization sequence, and some were incorporated within the whitlockite grain during its crystal growth process, resulting in droplets inclusion probably due to liquid immiscibility.

One small (30 μm across) isolated grain of potassium feldspar is found between the large crystals of plagioclase (Fig. 2e). Two grains of lath-shaped ilmenite, 100 μm and 170 μm across, crystallize with the Si, Al, K-rich glass and rims of Px 1 and Px 2 (Fig. 2c). The ilmenite contains 1 wt% of MgO. Tiny (<5 μm across) zircons precipitate

within the ilmenite.

3.2. *Troctolite*

The clast is a plagioclase-olivine cumulate and 2×1.8 mm in size (Fig. 6a). The texture is granoblastic with smooth curved grain boundaries. Due to the shock effect, plagioclase shows undulatory extinction and is partly intruded by dark glassy matrix. This clast dominantly includes subhedral to euhedral Mg-rich olivine (Fo=70) and Ca-rich plagioclase (An=95–97) with low-Ca pyroxene ($Wo_{3-11}Fs_{24-26}En_{73-63}$, mg#=71–75) filling interstices. Chemical compositions of plagioclase and olivine are fairly homogeneous, while pyroxene shows slight compositional variation (Figs. 7a–c). The accessory phases consist of a relatively large (200 μm across) FeNi metal, trace of Ti, Al-bearing chromite ($Chr_{64}Ulv_{10}Her_{26}$), ilmenite, troilite and apatite. Mineral compositions are shown in Table 3. The FeNi metal includes 6–7 wt% of Ni, which is

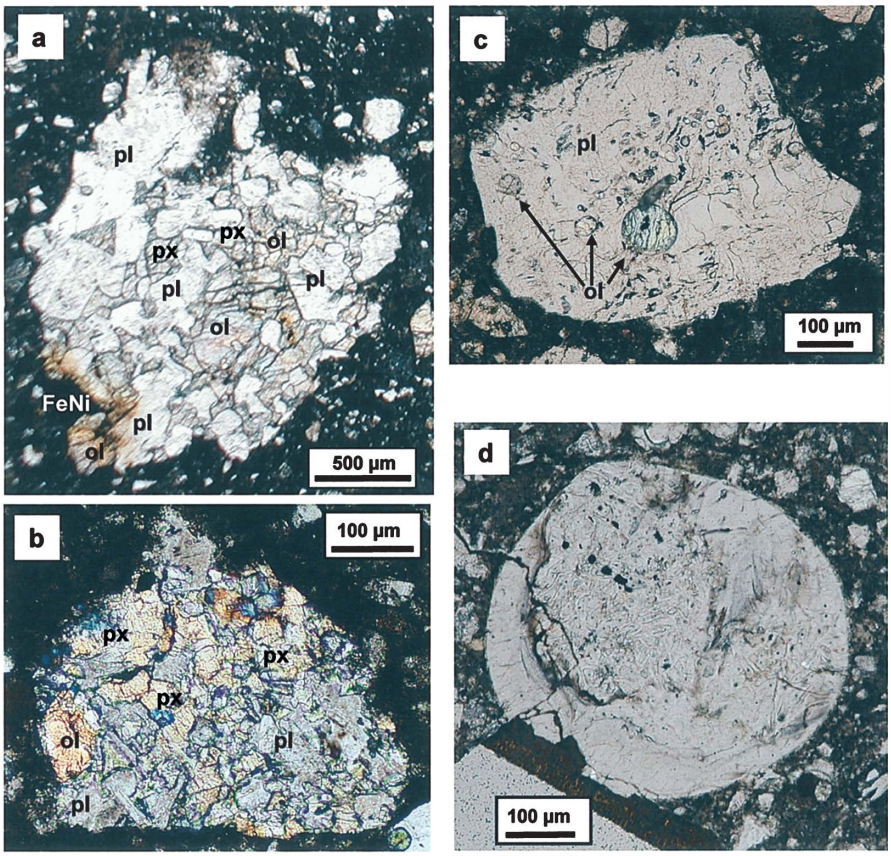

Fig. 6. a. Photomicrograph of troctolite. The clast is a plagioclase-olivine cumulate.
b. Photomicrograph of norite. The clast shows a fine-grained granoblastic texture with smooth curved grain boundary.
c. Photomicrograph of granulite. Olivines occur as round patches in a host plagioclase.
d. Photomicrograph of a large devitrified impact spherule.

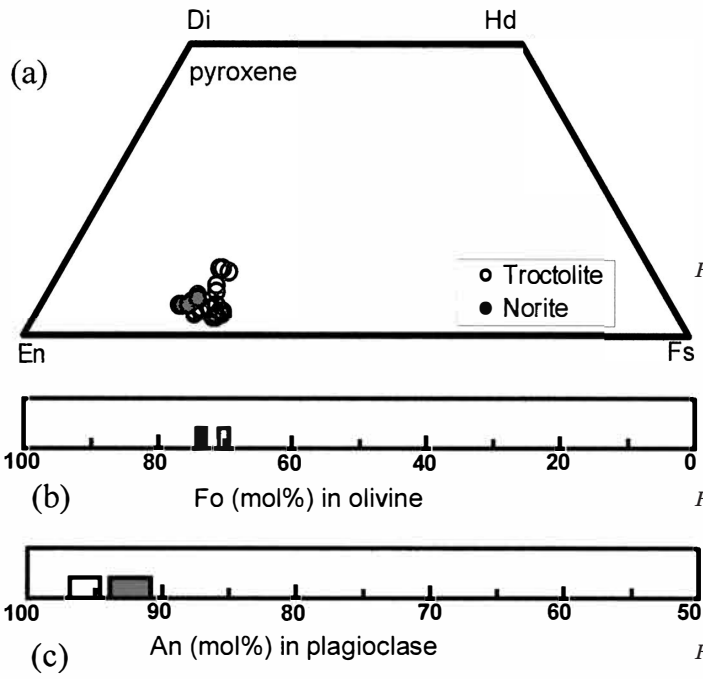

Fig. 7a. Pyroxene compositions of troctolite and norite plotted in the pyroxene quadrilateral.

Fig. 7b. Olivine compositions of troctolite and norite.

Fig. 7c. Plagioclase compositions of troctolite and norite.

marginally taenite. The apatite co-crystallizes with ilmenite, chromite, troilite and FeNi metal. The modal abundances are 60 vol% plagioclase, 23 vol% olivine and 16 vol% pyroxene (Table 1). Anorthositic norite might be appropriate for the clast due to the relatively low mode of plagioclase. Grain sizes of cumulative plagioclases range from 100 to 870 μm and the dominant ones are 200–400 μm, while those of olivines from 100 to 430 μm. All of the olivine grains are surrounded by pyroxene, and sub-rounded shapes and smooth-curved grain boundaries are indicative of "olivine-resorption" that the cumulative olivines react with the melt and later-crystallizing pyroxenes. The mg# of olivines (Fo = 70) and that of interstitial pyroxenes (mg# = 71–75) show the equilibration for olivine and pyroxene. The CaO content in olivines is 0.06 wt%, indicating the cooling rate is comparable to that of intrusive lunar olivines which is generally below 0.13 wt% (Papike *et al.*, 1998). FeO/MnO ratio of the olivine is 91, which falls within the range of typical lunar olivines (Papike *et al.*, 1998). Pyroxene includes small crystals of chromite. No detectable exsolution in pyroxene is observed. Smooth-curved grain boundaries, homogeneous mineral compositions and equilibrated mg#s in olivine and pyroxene, which are common features for lunar troctolites (*e.g.,* Dymek *et al.*, 1975), are all indicative of extensive subsolidus equilibration during slow cooling.

Due to the high Ni content (6–7 wt%) in the FeNi metal in contrast to less than 100 ppm of Ni in Apollo troctolites (*e.g.,* Papike *et al.*, 1998) the pristinity of this clast remains obscure.

Table 3. Mineral compositions of troctolite.

	Plagioclase	Olivine	Pyroxene			Cr-spinel		ilmenite		Apatite		FeNi	FeS
SiO_2	44.9	38.3	55.2	53.9		0.12	0.15	0.13	SiO_2	0.37	Fe	91.9	63.2
TiO_2	0.05	0.08	0.64	0.81		6.70	10.0	52.4	TiO_2	0.01	Ni	6.82	0.25
Al_2O_3	34.6	0.09	1.01	1.40		11.3	9.71	0.06	Al_2O_3	n.d.	S	0.01	35.7
FeO	0.29	26.7	15.8	16.2		30.4	32.4	37.6	FeO	1.04	Co	0.63	0.13
MnO	0.05	0.30	0.26	0.30		0.26	0.31	0.41	MnO	n.d.	Total	99.3	99.3
MgO	0.11	34.4	26.5	22.2		5.03	5.08	6.12	MgO	0.12			
CaO	19.0	0.06	1.58	5.28		0.25	0.14	0.28	CaO	53.7			
Na_2O	0.50	0.02	0.02	0.03		n.d.	n.d.	n.d.	Na_2O	n.d.			
K_2O	0.08	0.02	0.02	n.d.		n.d.	0.03	n.d.	K_2O	n.d.			
Cr_2O_3	0.03	0.08	0.32	0.54		47.0	42.0	1.17	Cr_2O_3	n.d.			
V_2O_3	n.d.	0.00	0.02	0.00		0.44	0.50	n.d.	V_2O_3	n.d.			
NiO	n.d.	0.01	0.02	0.07		0.05	0.03	n.d.	NiO	n.d.			
P_2O_5	n.d.	n.d.	0.05	n.d.		n.d.	0.02	n.d.	P_2O_5	40.9			
Total	99.6	100.0	101.5	100.8		101.6	100.4	98.2	Y_2O_3	n.d.			
									La_2O_3	0.06			
mg#		69.7	74.9	70.9	mg#	22.7	21.8	22.5	Ce_2O_3	n.d.			
Wo			3.1	10.8	Chr	61.4	55.6		Nd_2O_3	0.04			
Fs			24.3	25.9	Her	21.9	19.2		Cl	0.73			
En			72.6	63.3	Ulv	16.7	25.3		F	3.76			
Or	0.5								Total	99.0			
Ab	4.6												
An	95.0												

mg# = 100 × Mg/(Mg + Fe) mol ratio, Wo = 100 × Ca/(Ca +Fe +Mg) mol ratio, Fs = 100 × Fe/(Ca + Fe + Mg) mol ratio, En = 100 × Mg/(Ca + Fe + Mg) mol ratio
Or = 100 × K/(K + Ca + Na) mol ratio, Ab = 100 × Na/(K + Ca + Na) mol ratio, An = 100 × Ca/(K + Ca + Na) mol ratio.
Chr = 100 × Cr/(Cr + Al + 2 × Ti) mol ratio, Her = 100 × Al/(Cr + Al + 2 × Ti) mol ratio, Ulv = 100 × 2 × Ti/(Cr + Al + 2 × Ti) mol ratio. n.d. = not detected.

3.3. Norite

The clast, 0.4×0.3 mm in size, shows a fine-grained granoblastic texture with smooth curved grain boundary (Fig. 6b). Grain sizes of plagioclase and pyroxene seem less than 100 μm, although the original crystal shape appears to become ambiguous due to the smoothing. The pristinity of this clast is unsure because of the texture and grain size. It is composed of Ca-rich plagioclase (An=91–94), low-Ca pyroxene ($Wo_{5-7}Fs_{21-23}En_{74-70}$, Mg#=75–77), and Mg-rich olivine (Fo=74). Chemical composition of each phase is fairly homogeneous (Figs. 7a–c). Mineral composition is listed in Table 4. Modal abundance is 49 vol% plagioclase, 40 vol% pyroxene, and 11 vol% olivine (Table 1). No pyroxene exsolution is found. No accessory minerals and glasses are observed in this clast. The mg#s of pyroxene and olivine indicate they are equilibrated. Compared to the troctolite in this rock, the size of the clast and the grain size are much smaller, but the mg#s of the olivines and pyroxenes are higher than those in the troctolite.

Table 4. Mineral compositions of norite.

	Plagioclase		Olivine	Pyroxene	
SiO_2	45.5	46.2	39.2	55.5	55.0
TiO_2	n.d.	0.07	0.08	0.42	0.81
Al_2O_3	34.9	35.0	0.04	1.24	0.88
FeO	0.17	0.14	23.8	13.9	14.9
MnO	0.01	n.d.	0.24	0.26	0.30
MgO	0.08	0.06	37.3	26.1	25.3
CaO	18.4	18.3	0.14	2.44	3.26
Na_2O	0.60	0.94	n.d.	n.d.	0.02
K_2O	0.05	0.10	0.01	0.01	0.01
Cr_2O_3	0.02	n.d.	0.06	0.75	0.51
V_2O_3	n.d.	n.d.	0.04	n.d.	0.02
NiO	n.d.	n.d.	n.d.	0.06	0.01
P_2O_5	0.04	0.03	n.d.	0.01	0.02
Total	99.8	100.8	100.9	100.6	101.0
mg#			73.7	77.0	75.2
Wo				4.9	6.5
Fs				21.9	23.2
En				73.2	70.3
Or	0.3	0.6			
Ab	5.6	8.5			
An	94.1	90.9			

mg# = 100 × Mg/(Mg + Fe) mol ratio, Wo = 100 × Ca/(Ca +Fe +Mg) mol ratio,
Fs = 100 × Fe/(Ca + Fe + Mg) mol ratio, En = 100 × Mg/(Ca + Fe + Mg) mol ratio
Or = 100 × K/(K + Ca + Na) mol ratio, Ab = 100 × Na/(K + Ca + Na) mol ratio,
An = 100 × Ca/(K + Ca + Na) mol ratio. n.d. = not detected.

3.4. *High-Al basalt*

This clast, 1.2×0.7 mm in size, shows a fine-grained subophitic texture with plagioclase (An=91–97), olivine (Fo=66–70), pigeonite ($Wo_{11}Fs_{27}En_{62}$, mg#=70), augite ($Wo_{33}Fs_{22}En_{45}$, mg#=68), FeNi metal, troilite and apatite (Fig. 8). Mineral compositions are given in Table 5. The modal abundances are 75 vol% plagioclase, 11 vol% pyroxene and, and 11 vol% olivine (Table 1). Despite the subophitic texture, pyroxene composition does not show gradational zoning typical of rapidly cooled basalts, and instead, coexisting pigeonite and augite (Fig. 9a). Olivine and pyroxene crystallize interstitial to fine-grained laths of plagioclase, and some pyroxenes occur as overgrowth of olivines (Fig. 8b). Plagioclase and olivine compositions show slight

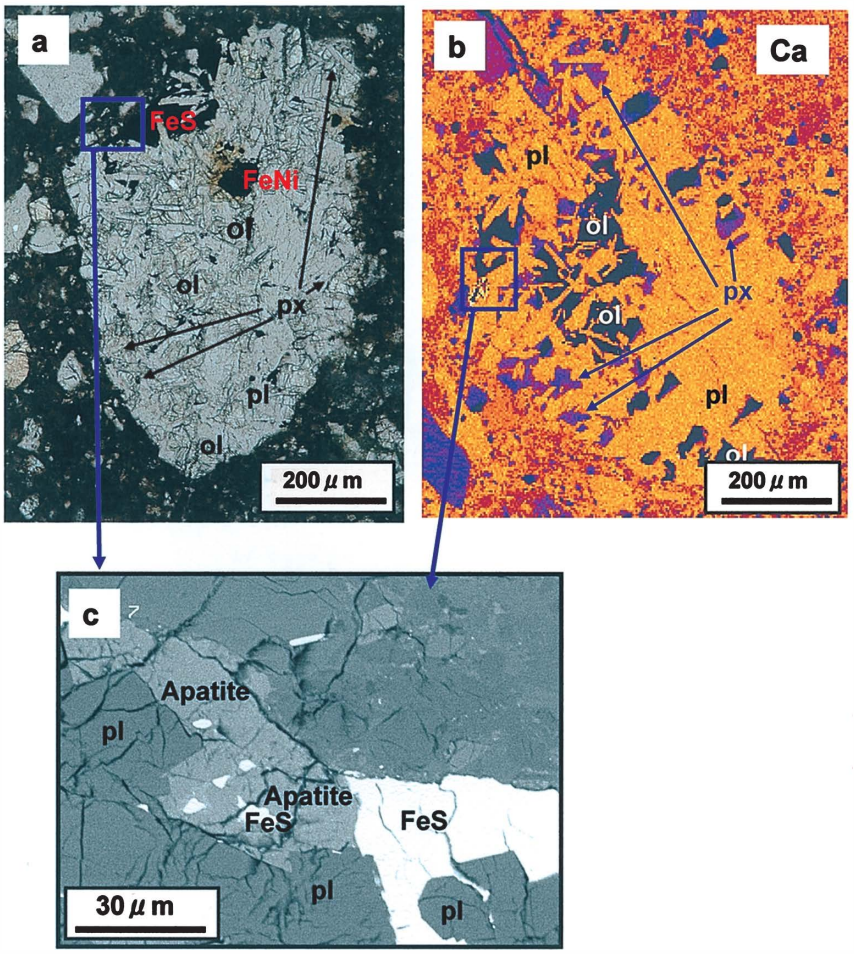

Fig. 8. a. Photomicrograph of high-Al basalt. The clast shows a fine-grained subophitic texture.
b. Ca map of high-Al basalt. Olivine and pyroxene crystallize interstitial to fine-grained laths of plagioclase, and some pyroxenes occur as overgrowth of olivines.
c. BSE image of coexisting apatite and troilite. Some troilite grains are found as inclusions within apatite.

Table 5. Mineral compositions of Hi-Al basalt.

	Plagioclase			Olivine		Pyroxene			Apatite		FeS	FeNi			
												Taenite 1		Taenite 2	
SiO_2	44.6	46.3	45.8	38.2	38.3	53.7	52.0	SiO_2	0.19	Fe	63.8	89.2	91.3	87.3	83.6
TiO_2	0.01	0.04	0.06	0.08	0.07	0.58	0.76	TiO_2	n.d.	Ni	0.11	8.83	6.09	9.39	13.4
Al_2O_3	35.2	35.1	31.8	0.13	0.03	2.09	1.67	Al_2O_3	0.01	S	36.1	n.d.	n.d.	n.d.	n.d.
FeO	0.17	0.62	1.05	27.3	30.1	16.4	13.0	FeO	0.53	Co	0.05	0.50	0.74	0.99	0.68
MnO	n.d.	n.d.	0.04	0.32	0.28	0.27	0.30	MnO	n.d.	Total	100.0	98.5	98.1	97.7	97.7
MgO	0.10	0.12	0.81	35.2	32.7	21.5	15.3	MgO	0.13						
CaO	19.1	18.9	17.4	0.25	0.23	5.22	15.5	CaO	54.8						
Na_2O	0.29	0.68	0.93	0.04	0.01	0.03	0.07	Na_2O	n.d.						
K_2O	0.04	0.09	0.09	n.d.	n.d.	n.d.	0.02	K_2O	n.d.						
Cr_2O_3	n.d.	0.01	0.07	0.14	0.17	0.94	0.90	Cr_2O_3	n.d.						
V_2O_3	n.d.	0.07	0.07	0.04	n.d.	0.09	n.d.	V_2O_3	n.d.						
NiO	n.d.	n.d.	0.03	0.06	n.d.	n.d.	n.d.	NiO	n.d.						
P_2O_5	n.d.	n.d.	n.d.	0.04	0.12	n.d.	n.d.	P_2O_5	40.9						
Total	99.5	102.0	98.2	101.8	102.1	100.8	99.5	Y_2O_3	n.d.						
								La_2O_3	0.08						
mg#				69.7	66.0	70.0	67.7	Ce_2O_3	0.23						
Wo						10.9	32.9	Nd_2O_3	0.10						
Fs						26.8	21.7	Cl	0.31						
En						62.4	45.4	F	3.49						
Or	0.2	0.5	0.6					Total	99.3						
Ab	2.7	6.1	8.7												
An	97.1	93.4	90.7												

mg# = 100 × Mg/(Mg + Fe) mol ratio, Wo = 100 × Ca/(Ca +Fe +Mg) mol ratio, Fs = 100 × Fe/(Ca + Fe + Mg) mol ratio, En = 100 × Mg/(Ca + Fe + Mg) mol ratio, Or = 100 × K/(K + Ca + Na) mol ratio, Ab = 100 × Na/(K + Ca + Na) mol ratio, An = 100 × Ca/(K + Ca + Na) mol ratio. n.d. = not detected.

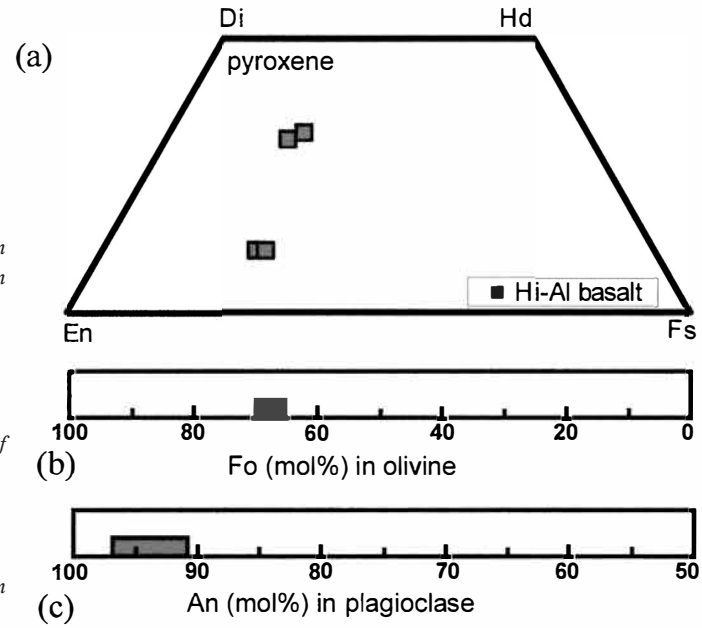

Fig. 9a. Pyroxene composition of high-Al basalt plotted in the pyroxene quadrilateral.

Fig. 9b. Olivine composition of high-Al basalt.

Fig. 9c. Plagioclase composition of high-Al basalt.

variations between grains (Table 5, Figs. 9b and 9c). Apatite crystallizes with troilite in mesostasis and some troilite grains are found as inclusions within apatite (Fig. 8c). Two grains of FeNi metal 50 μm in size, are both taenites with elevated content of Ni. The Ni concentration is heterogeneous within grains; one grain with Ni = 6.1–8.8 wt% and the other with Ni = 9.4–13.4 wt%. The high Ni content and intra-grain compositional variations of the FeNi metals imply the impact-melt derivation.

3.5. *Very low-Ti basalt*

This clast is 0.5 × 0.5 mm in size and consists of dominantly pyroxene and plagioclase with silica, fayalite, ilmenite and dark mesostasis (Fig. 10a). Radiate intergrowth of pyroxene and plagioclase is observed (Fig. 10b). Modal abundance is 53 vol% pyroxene and 43 vol% plagioclase (Table 1). Mineral compositions are given in Table 6. Pyroxene crystals show extensive chemical zoning from core to rim of the extremely Fe-rich augite (Figs. 10b and 11a). The compositional range of pyroxene is similar to that of Apollo 17 VLT basalts (Vaniman and Papike, 1977; Taylor *et al*., 1977), Luna 24 VLT ferrobasalts (Ryder and Marvin, 1978; Ma *et al*., 1978; Papike and Vaniman, 1978) and VLT basalt clasts in Antarctic lunar meteorites (Takeda *et al*., 1992; Arai *et al*., 1996, 2002; Arai and Warren, 1999; Mikouchi, 1999; Arai, 2001; Anand *et al*., 2003; Fagan *et al*., 2003). Plagioclase compositions are fairly homogeneous with An = 95–97 (Fig. 11b). Several silica minerals of 20–80 μm across are observed throughout the clast. The mesostasis areas adjacent to the Fe-rich augite rim show break-down of silica and fayalite with ilmenite and troilite (Fig. 10c). The texture of the clast and the strongly zoned pyroxene indicate rapid cooling typical of mare basalt.

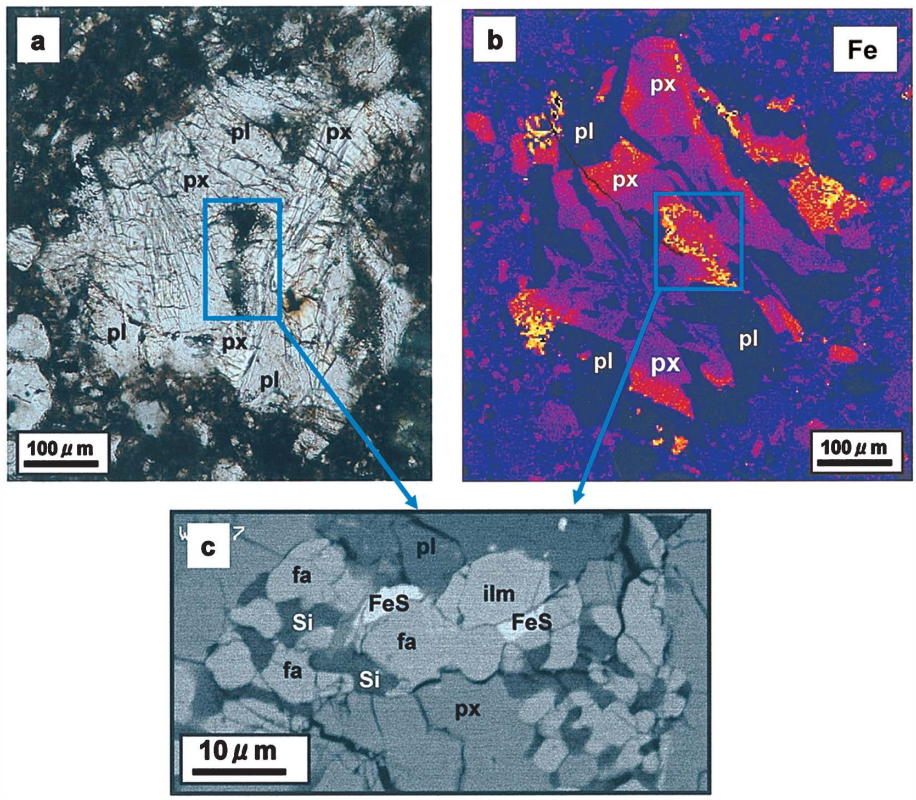

Fig. 10. a. Photomicrograph of VLT basalt.
b. Fe map of VLT basalt. Radiate intergrowth of pyroxene and plagioclase is observed.
c. BSE image of breakdown of silica and fayalite with ilmenite and troilite.

3.6. Granulite

Round, polygonal, olivine crystals with 30–200 μm in diameter are included in a 0.6×0.7 mm plagioclase crystal (Fig. 6c). Modal abundance is 91 vol% plagioclase and 9 vol% olivine (Table 1). Chemical compositions of olivine (Fo=69–71) and host plagioclase (An=95–96) are homogeneous (Table 7). Plagioclase shows undulatory extinction due to the shock effect. The modal abundance and mineral compositions show that the precursor of this granulite clast is ferroan anorthosite.

3.7. Glass spherules

Various size of glass spherules (50–500 μm across) are found in this PTS. Some are homogeneous in compositions, but others are devitrified and include plagioclase and pyroxene crystals (Fig. 6d). Chemical compositions of glass spherules without inclusions are fairly homogeneous, but compositional variations between spherules does exist; SiO_2=46.7–49.5 wt% and Al_2O_3=21.3–27.1 wt%, FeO=4.8–9.0 wt%, MgO=5.6–8.4 wt%, CaO=12.1–14.9 wt%, and Na_2O=0.13–0.62 wt%. Chemical compositions of homogeneous glasses are shown in Table 8. Provided these compositions that are

Table 6. Mineral compositions of VLT basalt.

	Plagioclase		Pyroxene		Ilmenite	Silica		FeS
			core	rim				
SiO_2	46.5	48.3	52.4	47.3	0.16	97.7	Fe	63.8
TiO_2	0.07	0.03	0.29	1.54	51.6	0.32	Ni	0.29
Al_2O_3	34.8	32.5	2.85	1.78	0.04	0.48	S	35.3
FeO	1.04	0.96	18.2	32.2	44.5	0.25	Co	0.05
MnO	0.00	0.06	0.43	0.47	0.44	0.09	Total	99.5
MgO	0.04	0.52	18.5	2.77	0.37	0.03		
CaO	19.1	18.0	6.84	12.3	0.31	0.25		
Na_2O	0.22	0.48	0.05	n.d.	n.d.	0.05		
K_2O	0.08	0.01	n.d.	0.02	n.d.	0.02		
Cr_2O_3	n.d.	0.04	0.90	0.25	0.44	0.00		
V_2O_3	0.02	n.d.	n.d.	n.d.	n.d.	0.07		
NiO	0.01	n.d.	0.06	n.d.	n.d.	n.d.		
P_2O_5	n.d.	n.d.	n.d.	0.04	0.02	0.02		
Total	101.9	100.9	100.4	98.6	97.8	99.2		
mg#			64.5	13.3	1.5			
Wo			14.6	29.7				
Fs			30.3	60.9				
En			55.1	9.3				
Or	0.5	0.1						
Ab	2.1	4.6						
An	97.4	95.4						

mg# = 100 × Mg/(Mg + Fe) mol ratio, Wo = 100 × Ca/(Ca +Fe +Mg) mol ratio,
Fs = 100 × Fe/(Ca + Fe + Mg) mol ratio, En = 100 × Mg/(Ca + Fe + Mg) mol ratio
Or = 100 × K/(K + Ca + Na) mol ratio, Ab = 100 × Na/(K + Ca + Na) mol ratio,
An = 100 × Ca/(K + Ca + Na) mol ratio. n.d. = not detected.

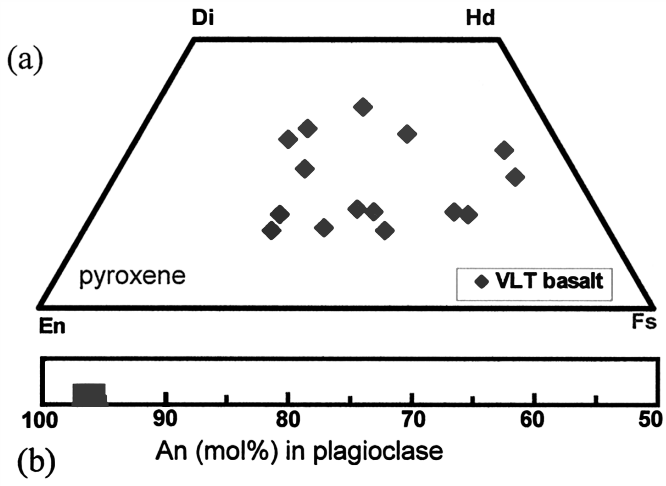

Fig. 11a. Pyroxene composition of VLT basalt plotted in the pyroxene quadrilateral.

Fig. 11b. Plagioclase composition of VLT basalt.

Table 7. Mineral compositions of granulite.

	Plagioclase	Olivine
SiO_2	45.1	38.2
TiO_2	0.03	0.00
Al_2O_3	35.4	0.00
FeO	0.09	26.9
MnO	0.06	0.34
MgO	0.12	34.7
CaO	18.8	0.10
Na_2O	0.38	0.01
K_2O	0.07	n.d.
Cr_2O_3	n.d.	0.17
V_2O_3	0.01	0.02
NiO	n.d.	0.04
P_2O_5	n.d.	n.d.
Total	100.1	100.5
mg#		70.0
Or	0.4	
Ab	3.5	
An	96.1	

mg# = 100 × Mg/(Mg + Fe) mol ratio
Or = 100 × K/(K + Ca + Na) mol ratio,
Ab = 100 × Na/(K + Ca + Na) mol ratio,
An = 100 × Ca/(K + Ca + Na) mol ratio.
n.d. = not detected.

Table 8. Chemical compositions of impact glasses.

	1	2	3
size (μm)	180	90	80
SiO_2	46.7	47.5	49.5
TiO_2	0.48	0.23	0.30
Al_2O_3	21.3	27.1	23.0
FeO	8.97	4.78	5.91
MnO	0.13	0.07	0.08
MgO	8.43	5.61	8.35
CaO	13.2	14.9	12.1
Na_2O	0.13	0.53	0.62
K_2O	0.08	0.03	0.04
Cr_2O_3	0.24	0.11	0.26
V_2O_3	0.01	0.01	0.01
NiO	0.03	0.02	0.00
P_2O_5	0.00	0.00	0.00
Total	99.7	101.0	100.2
Mg/Al	0.50	0.26	0.46

enriched in SiO_2 and Al_2O_3 and depleted in FeO and TiO_2, the glasses in Y983885 are apparently not of pyroclastic derivation, but of impact origin on highland terrane, based on the Delano's criteria (Delano, 1986). The intra-grain compositional variation represents the heterogeneous nature of a polymict regolith breccia.

4. Discussion

4.1. Petrogenesis of Y983885 KREEP basalt in relation to Apollo KREEP basalts

KREEP rocks have been considered geochemically and mineralogically uniform with following common traits: (1) basaltic texture, (2) moderate Fe/Mg ratio, despite the extremely high incompatible element abundance, (3) major element compositions saturated with low-Ca pyroxene (mostly orthopyroxene) and plagioclase. (4) uniform ratio of incompatible elements (*e.g.,* Warren *et al.*, 1983). KREEP basalts are found in Apollo15 and Apollo17 and small clasts in the impact melt breccia of Apollo 14, as well. Apollo 15 KREEP rocks have a wide range of textures from fasciculate to radiate, glomeroporphyritic, intersertal/intergranular to subophitic (Ryder, 1987). They consist of predominantly pyroxene and plagioclase with K-feldspar, ilmenite,

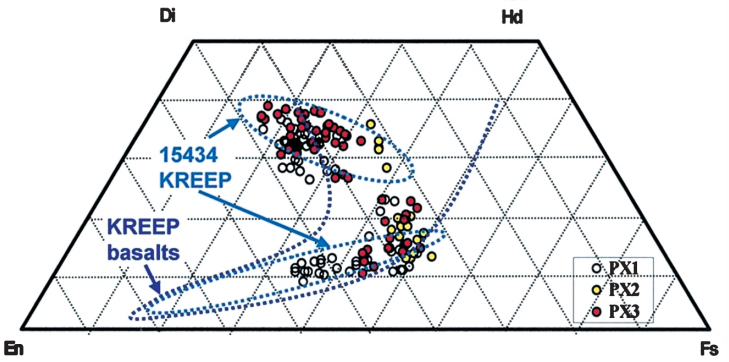

Fig. 12. Y983885 KREEP pyroxene composition in comparison with Apollo KREEP basalts. The pyroxene composition of the Apollo KREEP basalts (e.g., Ryder, 1976) is shown with a dotted purple envelope and that of the Apollo 15 15434 KREEP basalt (Vaniman and Papike, 1980) with dotted blue envelopes.

phosphate, silica mineral, troilite, FeNi metal, and glasses. Pyroxenes generally have cores of orthopyroxene overgrown by pigeonite and in turn by augite, displaying a gradual Ca-enrichment trend from orthopyroxene to pigeonite, and subsequently an abrupt increase of Ca from pigeonite to augite with some gap in the pyroxene quadrilateral (Fig. 12) (Ryder, 1976; Dowty *et al*., 1976; Meyer, 1977; Vaniman and Papike, 1980; Shervais and Vetter, 1989). In contrast, Apollo 17 KREEP basalts are subophitic to intersertal and do not contain orthopyroxene nor glassy mesostasis. Pyroxenes are zoned from relatively Fe-rich pigeonite core to Fe-rich augite rim which fall within the similar compositional range to those of Apollo 15 KREEP basalts (Ryder *et al*., 1975, 1977; Salpas *et al*., 1987). Plagioclase compositions are zoned from An＝90 to 70 (*e.g.,* Papike *et al*., 1998). Modal abundances in Apollo KREEP basalts are 40–43 vol% of plagioclase, 35–43 vol% of pyroxene and 8–20 vol% of glassy mesostasis (*e.g.,* Heiken *et al*., 1991).

The preserved igneous (subophitic ?) texture, primary chemical zonings in plagioclase and pyroxene and the presence of the glass mesostasis of Y983885 all suggest its rapid cooling history as an extrusive differentiate. However, the co-existing high-Ca pyroxene and low-Ca pyroxene and the submicron to micron-scale pyroxene exsolution are indicative of slower cooling than typical extrusive basalts, such as mare basalts (Arai and Warren, 1999). Yet, the chemical zonings in both high-Ca and low-Ca pyroxenes and the thickness of the pyroxene exsolution are not indicative of very slow cooling under plutonic condition, but of subsurface derivation, such as hypabyssal setting or lava pond. It is to be noted that the Y983885 plagioclase composition (An＝61–96) is more Na-enriched than those of known Apollo KREEP basalts (An＝70–90) (*e.g.*, Heiken *et al*., 1991), and comparable to those of quartz monzodiorites (An＝60–80), which is a coarse-grained variety of the KREEP (*e.g.,* Papike *et al*., 1998). Micron-scale of pyroxene exsolutions are also typical of quartz monzodiorites (*e.g.,* Ryder and Martinez, 1991). Despite the above mineralogical similarity to quartzs monzodiorite, the lack of compositional clustering by exsolved high-Ca and low-Ca pyroxenes, intergrowth of K-feldspar and silica minerals, and coarse grain size (*e.g.*, Ryder, 1976; Ryder and Martinez, 1991; Marvin *et al*., 1991) rule out the possibility that Y983885

KREEP clast is a quartz monzodiorite. The inferred extrusive (subsurface) derivation, chemical compositions of pyroxene and plagioclase, the presence of potassium feldspar, REE-rich whitlockite and more than 10 vol% of Si, Al, K-rich glass all indicate the clast is a KREEP basalt, though it was originally designated as alkali-rich rock (Arai *et al*., 2004). Although the bulk-clast incompatible trace element data primarily used as a criteria to distinguish KREEP is not available, it is almost certain that it is a KREEP basalt that is probably cooled slightly slower than the Apollo KREEP basalts, based on the mineralogical data.

Note that compositional variations of pyroxenes are mostly covered by the Apollo KREEP compositions (Fig. 12), but the zoning trend is unique in Y983885. The mineral mode is also distinct from Apollo KREEP basalts: 64 vol% of plagioclase in Y983885 *vs.* 40–43 vol% for Apollo KREEP. Primary orthopyroxenes and subsequent Ca zonings to pigeonite typical of Apollo KREEP basalts, are not present in this clast. Instead, the Y983885 KREEP basalt contains the co-existing pigeonite/augite (Px 1) and augite core/pigeonite rim (Px 2 and 3), both of which show chemical zonings and micron-scale exsolution. Vaniman and Papike (1980) reported the rare augite whose composition changes with Fe enrichment and minor Ca depletion in Apollo 15 KREEP basalt 15443 , which is partly similar to those in Y983885 KREEP basalt (Fig. 12). At this moment, it is unclear whether this unique trend found in this clast really represents a new trend distinct from the Apollo KREEP or just local heterogeneity in the similar trend to the Apollo KREEP basalt.

There is another mineralogical characteristics distinct from those of the Apollo KREEP basalts. The Y983885 KREEP basalt does not contain silica, fayalite, FeNi metal, and troilite as late crystallization stage phases, unlike typical Apollo KREEP basalts (*e.g.,* Papike *et al*., 1998). This might be due to sampling bias, but might be due to the following reason. The Si, Al, K rich glass, though it is compositionally heterogeneous, can theoretically yield about 45 vol% quartz and 55 vol% potassium feldspar. If the KREEP basalt would have been cooled more slowly probably far below the surface of lava or pluton, a silica mineral might have been precipitated from the Si, Al, K-rich glass. Immiscible silicate melts occur as a Fe-rich glass and a Si, K-rich one in Apollo 15 KREEP basalts (Hollister and Crawford, 1977; Crawford and Hollister, 1977). While the Si, K-rich glass is found in Y983885, the Fe-rich glass is not. This suggests a possibility that the Fe-rich melt to generate fayalite, FeNi metal and troilite might have been already removed by immiscible separation of mafic and felsic liquid. If that is a case, this KREEP basalt clast represents the mineral and glass assemblage right after the mafic liquid is physically separated from the Si, Al, K-rich liquid due to liquid immiscibility, but prior to the crystallization of silica from the felsic liquid.

However, the current mineralogical data available in the small clast are apparently not sufficient to draw any conclusion on the petrogenesis of this basalt. Further study of the additional samples is necessary to fully understand this new KREEP basalt.

4.2. Other clast lithologies in relation to Apollo samples and genetic association with KREEP

4.2.1. High-Al basalt

The high-Al basalts are mainly reported for Apollo 12 and 14 and characterized by

a wide range of incompatible trace element abundances, and have been divided into five groups on the basis of the REE abundances (Dickinson *et al*., 1985; Shervais *et al*., 1985). Note that bulk-rock major composition and mineralogy, do not considerably differ in each five group (Dickinson *et al*., 1985).

In order to explain the wide range of basalt compositions several petrogenetic models have been developed for the Apollo 14 high-Al basalts, (1) different degrees of partial melting of a source variably metasomatized by KREEP (Dickinson *et al*., 1985), (2) variable degrees of KREEP assimilation by the parent magma of the basalt group with the lowest REE abundance (Neal *et al*., 1988, 1989), and (3) impact melt origin (Snyder *et al*., 2000). The most recent study by Kramer and Neal (2003) concluded that petrogenesis of Apollo14 high-Al basalts could be modeled with three magmatic processes from one mantle source: partial melting of the Apollo14 basalt source, followed by fractional crystallization of the parental magma with and without simultaneous assimilation of KREEP. They also exclude the possibility of impact melt origin for Apollo 14 high-Al basalt based on their Ni data. Bulk-rock trace element data for Y983885 high-Al basalt is not available, but the presence of apatite (0.4 vol%) is indicative of enriched-REE concentration and likely genetic involvement with KREEP. Yet, with the enriched Ni content (Ni＝9.4–13.4 wt%) in the Fe-Ni metal, impact derivation of this high-Al basalt clast remains possible.

Apollo 14 high-Al basalts generally exhibit extensive chemical zonings of pyroxenes (*e.g.,* Dickinson *et al*., 1985; Shervais *et al*., 1985) with an exception of Apollo 14 14256 high-Al basalt which includes coexisting pigeonite and augite (Warner *et al*., 1980). The compositional clustering in the 14256 pyroxene is considered to reflect metamorphic nature of the sample (Warner *et al*., 1980). Thus, the co-existing pigeonite and augite without chemical zoning in Y983885 suggests the high-Al basalt are cooled rapidly enough to generate the subophitic texture, and subsequently annealed to equilibrate the primary compositional zoning of pyroxene, resulting in co-existing pigeonite and augite.

4.2.2. Mg-rich norite and troctolite

Mg-rich troctolites consist of three unbrecciated rocks from Apollo 17, and smaller troctolite clasts in the Apollo 14 breccias (Papike *et al*., 1998). Nearly all large norites are from Apollo 15 and 17 sites, and a few small fragments of norites have been identified from Apollo 14 site (Papike *et al*., 1998). They are characterized by high modal abundance of mafic minerals with high mg# and elevated incompatible and alkali element contents. A petrogenetic relationship between Mg-rich norites/troctolites and KREEP magmas has been strongly supported by recent intensive ion probe studies. Based on the parent melt compositions calculated from REE abundances of the pyroxene core compositions in Mg-rich norites (Papike *et al*., 1994, 1996) and troctolites (Shervais and McGee, 1998), the parent magma in equilibrium with the pyroxene cores are similar to medium- to high-K KREEP.

Apatite in Y983885 troctolite is indicative of association with KREEP. Future ion probe studies on the REE abundance of pyroxene core in these unique troctolite and norite will provide the additional data of the parent melt composition for the diverse Mg-rich rocks and validate their connection to KREEP.

In comparison with Apollo troctolites, the grain sizes of Y983885 troctolite are much smaller than those (2 to 3 mm) of typical troctolites, and the texture is analogous

to that of Apollo 14 granoblastic troctolite clasts, rather than Apollo 17 coarse-grained troctolite. The Mg# of the olivines (Fo=70) is much lower than that of a large (155 g) unbrecciated troctolite 76535 from Apollo 17 site (Fo=87–89) (Dymek *et al*., 1975) and even lower than Fe-rich olivine (Fo=77) in troctolite clasts in Apollo 14 impact melt breccias (*e.g.,* Warren *et al*., 1981; Shervais *et al*., 1983; Lindstrom, 1984). The mg# is so low that it is overlapped with the Mg-rich end of ranges of ferroan anorthosites (Heiken *et al*., 1991). However, we consider the clast belongs to Mg-rich lithology rather than ferroan anorthosite, based on the much lower modal abundance of plagioclase, compared to that of ferroan anorthosite with 83–99 vol% (Papike *et al*., 1998).

The grain sizes of Y983885 norite are also by far smaller than Apollo samples (over 1 mm to 1 cm), and the mg# of the pyroxenes (Fo=70) is lower, close to the lowest mg# (Fo=71–83) in Apollo norites (Papike *et al*., 1998). The modal abundance of olivine in the norite is much higher, reaching 11 vol%, compared to 1 vol% of rare olivine in norite clasts in Apollo 14 impact melt breccias. Note that Apollo 15 and 17 coarse-grained norites are free of olivine (Papike *et al*., 1998). The mg# of olivine (Fo=74) is comparable to those of Apollo 14 norite clasts (Fo=71 and 74) (Papike *et al*., 1998). Due to the paucity or the extremely low value (1 vol%) of modal olivine in Apollo norites, it has been suggested that there is no rock type with gradation in mode from norite to troctolite (Papike *et al*., 1998). The presence of the norite with relatively high modal olivine in Y983885 supports the existence of a rock type with intermediate modal abundance between norite and troctolite. Furthermore, the less magnesian pyroxene and olivine in troctolite and norite than in known Apollo norites and troctolites suggests lateral and/or vertical variability in modal abundances and mafic mineral compositions for the Mg-rich lithologies.

4.2.3. VLT basalt

VLT basalts have been found as only small fragments in Apollo 17 (Vaniman and Papike, 1977; Taylor *et al*., 1977) and Luna 24 samples (Ryder and Marvin, 1978; Ma *et al*., 1978), and in several brecciated lunar meteorites (Takeda *et al*., 1992; Arai *et al*., 1996, 2002; Arai and Warren, 1999; Mikouchi, 1999; Arai, 2001; Anand *et al*., 2003; Fagan *et al*., 2003; Jolliff *et al*., 2003). The genetic relationship with KREEP has been recently focused for fragmental breccias EET87521/EET96008 (Anand *et al*., 2003; Korotev *et al*., 2003) and a dimict breccia NWA 773 (Fagan *et al*., 2003; Jolliff *et al*., 2003). Korotev *et al*. (2003) suggested possible assimilation of a KREEP-bearing crustal component by a VLT basaltic magma or incorporation of the KREEP component in the mantle by retention of trapped melt in the mantle cumulate, based on the evolved components in EET87521/EET96008 with relative concentrations of incompatible elements similar to those of KREEP. NWA 773 consists of a VLT basaltic breccia and an olivine-gabbro cumulate, and it is inferred from the compositional similarities and petrogenetic modeling that the parent melt for the olivine-gabbro cumulate would be the VLT magma that incorporated KREEP (Fagan *et al*., 2003; Jolliff *et al*., 2003).

Y983885 includes a VLT basalt and troctolite/norite. Since the VLT basalt does not contain phosphate nor potassium feldspar as in other known VLT basalts, a direct association with KREEP, such as the assimilation by KREEP in the case of high-Al basalt is unlikely. However, genetic connection as a source for troctolite/norite as

inferred for NWA 773, might be the case. Otherwise, the VLT basalt might be an exotic component which is transported from a distant mare region. Further studies on trace element characteristics both for VLT basalt and troctolite/norite are required to verify their genetic relationship and association with KREEP.

4.3. Enrichment of Na and Si in the impact glasses

Since impact glasses can be considered as a fused material of a target region, the homogeneous glass compositions are expected to represent a bulk-regolith composition of the impact target area, possibly near the source region of this meteorite. Comparing with the bulk-rock compositions of the known feldspathic lunar meteorite breccias (Warren and Kallemeyn, 1991; Korotev *et al*., 2003), Y983885 glass compositions are distinguished with an exceptionally high SiO_2 and Na_2O content in Glass 2 and 3 of Table 8. While feldspathic highland lunar meteorites generally contain 43.5–48 wt% of SiO_2 and 0.27–0.43 wt% of Na_2O (Warren and Kallemeyn, 1991; Korotev *et al*., 2003), Y983885 glass 3 includes 49.5 wt% of SiO_2 and 0.62 wt% of Na_2O. The enrichment of SiO_2 and Na_2O in the impact glasses might reflect relatively high abundance of these elements in the local regolith, possibly due to the presence of higher-silica KREEP basalt, granite and quartz monzodiorite in the source region.

4.4. Relationship with other lunar meteorites

Y983885 is the first lunar meteorite which contains the clast of an igneous KREEP basalt. The meteorite also includes prominent clast lithologies, which are genetically associated with KREEP. There are many anorthositic regolith breccias which include clasts of ferroan anorthosite and Mg-rich rock, but none of them includes an igneous KREEP basalt. There is one lunar meteorite which is extremely enriched in KREEP composition. An impact-melt breccia, Sayh al Uhaymir (SaU) 169 has a chemical composition similar to Apollo KREEP impact melt with the highest concentration in KREEP elements among all the lunar rocks to date, and is suggested to be derived from one of the Th hot spot on the Procellarum KREEP terrane (Gnos *et al*., 2004). Due to the impact-melt nature of the SaU 169, primary mineralogical and geochemical characteristics during the KREEP volcanism are unfortunately not preserved. Antarctic lunar meteorites with VLT basalt clasts are dominantly composed of mare components (Takeda *et al*., 1992; Arai *et al*., 1996, 2002; Arai and Warren, 1999; Mikouchi, 1999; Arai, 2001; Anand *et al*., 2003; Fagan *et al*., 2003; Jolliff *et al*., 2003) and unlikely share a common derivation with Y983885.

4.5. Possible source region on the Moon

A variety of crustal rocks genetically associated with KREEP distinguish Y983885 from other lunar meteorites. Y983885 is also characterized by SiO_2 and Na_2O-enriched impact glasses which infer high Si, Na concentration of the source region, possibly reflecting relatively high abundance of alkali-rich evolved rocks, such as higher-silica KREEP basalt, granite and quartz monzodiorite. Apollo 14 polymict regolith breccias have been reported to distinctly have clasts of KREEP basalts, Mg-rich rocks, alkali-rich rocks, high-Al basalts, and evolved lithologies, such as granites and felsites (*e.g.,* Hunter and Taylor, 1983; Shervais *et al*., 1983, 1985). Apollo 14 sites, known as Fra

Mauro Formation, are geologically unique among other Apollo sites because the bedrock consists of indulated polymict breccia, which probably represents material entrained by impacts related to the Imbrium event (Warren *et al*., 1983). The Lunar Prospector γ-ray mapping demonstrated that near-side Procellarum terrane in the northwestern hemisphere (Apollo12–14 region) is exceptionally enriched in the incompatible trace elements, such as KREEP (*e.g.,* Wieczorek *et al*., 1999). Simultaneous occurrence of clasts of a KREEP basalt and genetically KREEP-related, high-Al basalt, a Mg-rich troctolite/norite and the impact glasses relatively enriched in Si and Na in Y983885 can constrain the source region of the meteorite to the KREEP-enriched Procellarum terrane. Further studies on the bulk-rock composition and trace element/isotopic composition of minerals in the each clast will provide additional constraints on the petrogenesis and the associations to KREEP.

5. Conclusion

Y983885 is a polymict regolith breccia with prominent clast lithologies and relatively Si, Na-rich impact spherules. A variety of clasts consist of a KREEP basalt, a Mg-rich troctolite, a Mg-rich norite, a high-Al basalts, a very low-Ti basalt, and a granulite originated from ferroan anorthosite. Note that an igneous KREEP basalt is first reported in this lunar meteorite. The KREEP basalt clast consists of ternary plagioclase, pigeonite, augite, REE-rich whitlockite, ilmenite, Si, Al, K-rich glass, and Ba-rich potassium feldspar. The KREEP basalt is mineralogically distinct from Apollo KREEP basalts: (1) lack of the typical Ca zoning from orthopyroxene to pigeonite instead, the presence of the co-existing pigeonite/augite and augite core/pigeonite rim, both of which show chemical zonings and micron-scale exsolution and (2) the extremely Na and K-enriched plagioclase ($An_{68}Ab_{29}Or_3$–$An_{61}Ab_{36}Or_3$), which is more evolved than that in KREEP basalt (An = 70–90), and comparable to that in quartz monzodiorites (An = 60–80), and (3) lack of silica, fayalite, troilite, FeNi metal in the late stage product. With these mineral characteristics, a KREEP basalt is probably cooled slightly slower than the Apollo KREEP basalts, under the subsurface condition such as hypabyssal setting or lava pond. However, it is kept in mind the current mineralogical data available in the small clast are apparently not sufficient and further study of the additional samples is necessary to fully understand the petrogenesis of this new KREEP basalt.

The troctolite and norite in Y983885 are also unique in low mg# of mafic minerals and higher modal abundance of olivine in norite and, comparing to Apollo troctolites and norites. The higher modal abundance of olivine in the norite implies the possible existence of a rock type with intermediate modal abundance between norite and troctolite, and the presence of mafic minerals with lower mg# than those in Apollo troctolites and norites, represents the compositional diversity of Mg-rich lithologies. Simultaneous occurrence of clasts of a KREEP basalt and genetically KREEP-related, high-Al basalt, a Mg-rich troctolite/norite and the impact glasses relatively enriched in Si and Na in Y983885 can constrain the source region of the meteorite to the KREEP-enriched Procellarum terrane in the northwestern hemisphere of the lunar nearside.

Further studies on the bulk-rock composition and trace element/isotopic composi-

tion of minerals in the each clast will provide additional constraints on the petrogenesis of and the associations to KREEP of this significant lunar meteorite.

Acknowledgements

We are grateful to NIPR for providing the sample. We thank Drs. J.J. Papike and A. Yamaguchi for constructive reviews that significantly improved the manuscript.

References

Anand, M., Taylor, L.A., Neal, C.R., Snyder, G.A., Patchen, A., Sano, Y. and Terada, K. (2003): Petrogenesis of lunar meteorite EET 96008. Geochim. Cosmochim. Acta, **67**, 3499–3518.

Arai, T. (2001): Mineralogical study of lunar mare meteorite EET 96008. Antarctic Meteorites XXVI. Tokyo, Natl Inst. Polar Res., 3–6.

Arai, T. and Warren, P.H. (1999): Lunar meteorite QUE94281: Glass compositions and other evidence for launch pairing with Yamato793274. Meteorit. Planet. Sci., **34**, 209–234.

Arai, T., Takeda, H. and Warren, P.H. (1996): Four lunar mare meteorites: Crystallization trends of pyroxene and spinels. Meteorit. Planet. Sci., **31**, 877–892.

Arai, T., Ishii, T. and Otsuki, M. (2002): Mineralogical study of lunar mare meteorite Yamato 981031. Lunar and Planetary Science XXXIII. Houston, Lunar Planet. Inst., Abstract #2064 (CD-ROM).

Arai, T., Otsuki, M., Ishii, T., Mikouchi, T. and Miyamoto, M. (2004): Mineralogy of Yamato 983885 lunar polymict breccia with alkali-rich and Mg-rich rocks. Lunar and Planetary Science XXXV. Houston, Lunar Planet. Inst., Abstract #2155 (CD-ROM).

Bence, A.E. and Albee, A.L. (1968): Empirical correction factors for the electron microanalysis of silicates and oxides. J. Geol., **76**, 382–403.

Bence, A.E. and Papike, J.J. (1972): Pyroxenes as recorders of lunar basalt petrogenesis; Chemical trends due to crystal-liquid interaction. Proc. Lunar Sci. Conf., **3rd**, 431–469.

Crawford, M.L. and Hollister, L.S. (1977): Evolution of KREEP: Further petrologic evidence. Proc. Lunar Sci. Conf., **8th**, 2403–2417.

Delano, J.W. (1986): Pristine volcanic glasses; Criteria, data and implications. Proc. Lunar Planet. Sci. Conf., **16th**, Pt. 2, D201-D213 (J. Geophys. Res., **91**, B4).

Dickinson, T., Taylor, G.J., Keil, K., Schmitt, R.A., Hughes, S.S. and Smith, M.R. (1985): Apollo 14 aluminous mare basalts and their possible relationship to KREEP. Proc. Lunar Planet. Sci. Conf., **15th**, Pt. 2, C365-C374 (J. Geophys. Res., **90** Suppl.).

Dowty, E., Keil, K., Prinz, M., Gros, J. and Takahashi, H. (1976): Meteorite-free Apollo 15 crystalline KREEP. Proc. Lunar Sci. Conf., **7th**, 1833–1844.

Dymek, R.F., Albee, A.L. and Chodos, A.A. (1975): Comparative petrology of lunar cumulate rocks of possibly primary origin: Dunite 72415, troctolite 76535, norite 78235 and anorthosite 62337. Proc. Lunar Sci. Conf., **6th**, 301–341.

Gnos, E., Hofmann, B.A., Al-Kathiri, A., Lorenzetti, S., Eugster, O., Whitehouse, M.J., Villa, I.M., Jull, A. J.T., Eikenberg, J., Spettel, B., Krähenbühl, U., Franchi, I.A. and Greenwood, R.C. (2004): Pinpointing the source of a lunar meteorite: Implications for the evolution of the Moon. Science, **305**, 657–659.

Fagan, T.L., Keil, K., Taylor, G.J., Hicks, T.L., Killgore, M. *et al*. (2003): Northwest Africa 773: Lunar origin and iron-enrichment trend. Meteorit. Planet. Sci., **38**, 529–554.

Heiken, G.H., Vaniman, D.T. and French, B.M., ed. (1991): Lunar Sourcebook: A User's Guide to the Moon. Cambridge, Cambridge Univ. Press.

Hollister, L.S. and Crawford, M.L. (1977): Melt immiscibility in Apollo 15 KREEP: Origin of Fe-rich mare basalts. Proc. Lunar Sci. Conf., **8th**, 2419–2432.

Hunter, R.H. and Taylor, L.A. (1983): The magma ocean from the Fra Mauro shoreline: An overview of the Apollo 14 crust. Proc. Planet. Sci. Conf., **13th**, Pt. 2, A591–A602 (J. Geophys. Res., **88** Suppl.)

Jolliff, B.L. (1991): Fragments of quartz monzodiorite and felsite in Apollo 14 soil particles. Proc. Lunar Planet. Sci., **21**, 101–118.

Jolliff, B.L., Korotev, R.L., Zeigler, R.A. and Floss, C. (2003): Northwest Africa 773: Lunar mare breccia with a shallow-formed olivine-cumulate components, inferred very-low-Ti (VLT) heritage, and a KREEP connection. Geochim. Cosmochim. Acta, **67**, 4857–4879.

Kaiden, H. and Kojima, H. (2002): Yamato 983885: A new lunar meteorite found in Antarctica. Lunar and Planetary Science XXXIII. Houston, Lunar Planet. Inst., Abstract #1958 (CD-ROM).

Korotev, R.L., Jolliff, B.L., Zeigler, R.A and Haskin, L.A. (2003): Compositional constraints on the launch pairing of three brecciated lunar meteorites of basaltic composition. Antarct. Meteorite Res., **16**, 152–175.

Kramer, G.Y. and Neal, C.R. (2003): Petrogenesis of the Apollo 14 high-Al basalts revisited: distinct magmatic event, source metasomatism, and AFC. Lunar and Planetary Science XXXIV. Houston, Lunar Planet. Inst., Abstract #2035 (CD-ROM).

Lindstrom, M.M. (1984): Alkali gabbronorite, ultra-KREEPy melt rock and the diverse suite of clasts in North Ray Crater feldspathic fragmental breccia 67975. Proc. Lunar Planet. Sci. Conf., **15th**, Pt. 1, C50–C62 (J. Geophys. Res., **89** Suppl.).

Ma, M.-S., Schmitt, R.A., Taylor, J.G., Warner, R.D., Lange, D.E. and Keil, K. (1978): Chemistry and petrology of Luna 24 lithic fragments and $<250\,\mu$m soils; Constraints on the origin of VLT mare basalts. Mare Crisium: The View from Luna 24, ed. by R.B. Merrill and J.J. Papike. New York, Pergamon, 569–592,.

Marvin, U.B., Lindstrom, M.M., Holmberg, B.B. and Martinez, R.R. (1991): New observations on the quartz monzodiorite-granite suite. Proc. Lunar Planet. Sci., **21**, 119–135.

Meyer, C., Jr. (1977): Petrology, mineralogy and chemistry of KREEP basalt. Phys. Chem. Earth, **10**, 239–260.

Mikouchi, T. (1999): Mineralogy and petrology of a new lunar meteorite EET96008: Lunar basaltic breccia similar to Y-79327, QUE94281 and EET87521. Lunar and Planetary Science XXX. Houston, Lunar Planet. Inst., Abstract #1558 (CD-ROM).

Neal, C.R., Taylor, L.A. and Lindstrom, M.M. (1988): Apollo 14 mare basalt petrogenesis: Assimilation of KREEP-like components by a fractionating magma. Proc. Lunar Planet. Sci. Conf., **18th**, 139–153.

Neal, C.R., Taylor, L.A., Schmitt, R.A., Hughes, S.S. and Lindstrom, M.M. (1989): High alumina (HA) and very high potassium (VHK) basalt clasts from Apollo 14 breccias, Part 2. Whole rock geochemistry: Further evidence of combined assimilation and fractional crystallization within the lunar crust. Proc. Lunar Planet. Sci. Conf., **19th**, 147–161.

Papike, J.J. and Vaniman, D.T. (1978): Luna 24 ferrobasalts and the mare basalt suite: Comparative chemistry, mineralogy, and petrology. Mare Crisium: The View from Luna 24, ed. by R.B. Merrill and J.J. Papike. New York, Pergamon, 371–401.

Papike, J.J., Fowler, G.W. and Shearer, C.K. (1994): Orthopyroxenes as a recorder of lunar Mg-suite norite petrogenesis: an ion microprobe investigation of Mg-suite norites. Am. Mineral., **79**, 796–800.

Papike, J.J., Fowler, G.W., Shearer, C.K. and Layne, G.D. (1996): Ion microprobe investigation of plagioclase and orthopyroxene from lunar Mg-suite norites: Implications for calculating parental melt REE concentrations and for assessing postcrystallization REE redistribution. Geochim. Cosmoochim. Acta, **60**, 3967–3978.

Papike, J.J., Ryder, G. and Shearer, C.K. (1998): Lunar samples. Reviews in Mineralogy, Vol. 36, Planetary Materials, ed. J.J. Papike. Washington, D.C., Mineral. Soc. Am., 5-1–5-234.

Ryder, G. (1976): Lunar sample 15405: Remnant of a KREEP basalt-granite differentiated pluton. Earth Planet. Sci. Lett., **29**, 255–268.

Ryder, G. (1987): Petrographic evidence of nonlinear cooling rates and volcanic origin for Apollo 15 KREEP basalts. Proc. Lunar Sci. Conf., **17th**, Pt. 2, E331–E339 (J. Geophys. Res., **92**, B4).

Ryder, G. and Marvin, U.B. (1978): On the origin of Luna 24 basalts and soils. Mare Crisium: The View from Luna 24, ed. by R.B. Merrill and J.J. Papike. New York, Pergamon, 339–356.

Ryder, G. and Martinez, R.R. (1991): Evolved hypabyssal rocks from station 7, Apennine Front, Apollo 15. Proc. Lunar Planet. Sci., **21**, 137–150.

Ryder, G., Stoeser, D.B., Marvin, U.B., Bower, J.F. and Wood, J.A. (1975): Boulder 1, Station 2, Apollo17:

Petrology and petrogenesis. The Moon, **14**, 327–357.
Ryder, G., Stoeser, D.B., and Wood, J.A. (1977): Apollo17 KREEPy basalt: A rock type intermediate between KREEP and mare basalts. Earth Planet. Sci. Lett., **35**, 1–13.
Salpas, P.A., Taylor, L.A., Lindstrom, M.M. (1987): Apollo 17 KREEPy basalts: Evidence for the non-uniformity of KREEP. Proc. Lunar Planet. Sci. Conf., **17th**, Pt. 2, E340–E348 (J. Geophys. Res., **92**, B4).
Shervais, J.W. and McGee, J.J (1998): Ion and electron microprobe study of troctolites, norite, and anorthosites from Apollo 14: Evidence for urKREEP assimilation during petrogenesis of Apollo 14 Mg-suite rocks. Geochim. Cosmochim. Acta, **62**, 3009–3023.
Shervais, J.W. and McGee, J.J (1999): KREEP cumulates in the western lunar highlands: Ion and electron microprobe study of alkali-suite anorthosites and norites from Apollo 12 and 14. Am. Mineral., **84**, 806–820.
Shervais, J.W. and Vetter, S.K. (1989): Melt rock components in KREEPy breccia 15205-petrography and mineral chemistry of KREEP basalts and quartz-normative mare basalts. Lunar and Planetary Science XX. Houston, Lunar Planet. Inst., 1000–1001.
Shervais, J.W., Taylor, L.A. and Laul, J.C. (1983): Ancient crustal components in Fra Mauro breccias. Proc. Planet. Sci. Conf., **14th**, Pt. 1, B177–B192 (J Geophys. Res., **88** Suppl.).
Shervais, J.W., Taylor, L.A. and Lindstrom, M.M. (1985): Apollo 14 mare basalts: Petrology and geochemistry of clasts from consortium breccia 14321. Proc. Planet. Sci. Conf., **15th**, Pt. 2, C375–C395 (J. Geophys. Res., **90** Suppl.).
Snyder, G.A., Taylor, L.A. and Halliday, A.N. (1995a): Chronology and petrogenesis of the lunar highlands alkali suite: Cumulates from KREEP basalt crystallization. Geochim. Cosmochim. Acta, **59**, 1185–1203.
Snyder, G.A., Neal, C.R., Taylor, L.A. and Halliday, A.N. (1995b): Processes involved in the formation of magnesian-suite plutonic rocks from highlands of the Earth's Moon. J. Geophys. Res., **100** (E5), 9365–9388.
Snyder, G.A., Borg, L.E., Nyquist, L.E. and Taylor, L.A. (2000): Chronology and isoopic constraints on lunar evolution. Origin of the Earth and Moon, ed, by R.M. Canup and K. Righter. Tucson, Univ. Arizona Press, 361–395.
Takeda, H., Mori, H., Saito, J. and Miyamoto, M. (1992): Mineralogical studies of lunar mare meteorites EET 87521 and Y 793274. Lunar and Planetary Science XXII. Houston, Lunar Planet. Inst., 355–364.
Taylor, J.G., Keil, K. and Warner, R.D. (1977): Very low-Ti mare basalts. Geophys. Res. Lett., **4**, 207–210.
Vaniman, D.T. and Papike, J.J. (1977): Very low-Ti (VLT) basalts: A new mare rock type from the Apollo 17 drill core. Proc. Lunar Sci. Conf., **8th**, 1443–1471.
Vaniman, D.T. and Papike, J.J. (1980): Lunar highlan melt rocks: Chemistry, petrology and silicate mineralogy. Proc. Conf. Lunar Highlands Crust, 271–337.
Warner, R.D., Taylor, J.G., Keil, K., Ma, M.-S. and Schmitt, R.A. (1980): Aluminous mare basalts; New data from Apollo 14 coarse fines. Proc. Lunar Planet. Sci. Conf., **11th**, 87–104.
Warren, P.H. and Kallemeyn, G.W. (1991): Geochemical investigations of five lunar meteorirtes: Implications for the composition, origin and evolution of the lunar crust. Proc. NIPR Symp. Antarct. Meteorites, **4**, 91–117.
Warren, P.H., Taylor, G.J., Keil, K., Marshall, C. and Wasson, J.T. (1981): Foraging westward for pristine non-mare rocks: Complications for petrologic models. Proc. Lunar Planet. Sci., **12B**, 21–40.
Warren, P.H., Taylor, G.J., Keil, K., Kallemeyn, G. W., Shirley, D.N. and Wasson, J.T. (1983): Seventh foray: whitlockite-rich lithologies, a diopside-bearing troctolitic anorthosite, ferroan anorthosites, and KREEP. Proc. Lunar Planet. Sci. Conf., **14th**, Pt. 1, B151-B164 (J. Geophy Res., **88** Suppl.).
Wieczorek, M.A., Pahillips, R.J., Korotev, R.L., Jolliff, B.J. and Haskin, L.A. (1999): Geophysical evidence for the existence of the lunar "Procellarum KREEP Terrane". Lunar and Planetary Science XXX. Houston, Lunar Planet. Inst., Abstract #1548 (CD-ROM).